

An Oscillatory Contractile Pole-Force Component Dominates the Traction Forces Exerted by Migrating Amoeboid Cells

BALDOMERO ALONSO-LATORRE,¹ JUAN C. DEL ÁLAMO,¹ RUEDI MEILI,² RICHARD A. FIRTEL,²
and JUAN C. LASHERAS¹

¹Department of Mechanical and Aerospace Engineering, University of California, San Diego, 9500 Gilman Dr., La Jolla, CA 92093, USA; and ²Section of Cell and Developmental Biology, Division of Biological Sciences, University of California, San Diego, 9500 Gilman Dr., La Jolla, CA 92093, USA

(Received 29 March 2011; accepted 11 June 2011; published online 29 June 2011)

Associate Editor Edward Guo oversaw the review of this article.

Abstract—We used principal component analysis to dissect the mechanics of chemotaxis of amoeboid cells into a reduced set of dominant components of cellular traction forces and shape changes. The dominant traction force component in wild-type cells accounted for ~40% of the mechanical work performed by these cells, and consisted of the cell attaching at front and back contracting the substrate towards its centroid (pole-force). The time evolution of this pole-force component was responsible for the periodic variations of cell length and strain energy that the cells underwent during migration. We identified four additional canonical components, reproducible from cell to cell, overall accounting for an additional ~20% of mechanical work, and associated with events such as lateral protrusion of pseudopodia. We analyzed mutant strains with contractility defects to quantify the role that non-muscle Myosin II (MyoII) plays in amoeboid motility. In MyoII essential light chain null cells the polar-force component remained dominant. On the other hand, MyoII heavy chain null cells exhibited a different dominant traction force component, with a marked increase in lateral contractile forces, suggesting that cortical contractility and/or enhanced lateral adhesions are important for motility in this cell line. By compressing the mechanics of chemotaxing cells into a reduced set of temporally-resolved degrees of freedom, the present study may contribute to refined models of cell migration that incorporate cell-substrate interactions.

Keywords—Cell migration, Traction forces, Dictyostelium, Principal component analysis, Chemotaxis, Myosin.

INTRODUCTION

Amoeboid cell migration is central to many physiological processes, including wound healing, immune response, or embryonic development.^{20,22,29,30} Its deregulation is a very important factor for serious pathological processes, as varied as tumor invasion, vascular diseases, or mental retardation.^{9,24,37} Cell migration requires the coordinated regulation of many molecules, but occurs through a small repertoire of shape changes consisting mainly of a sequence of anterior protrusions and posterior retractions.² There is ample evidence indicating that these morphological shape changes are mechanically coupled to the biochemical modulation of the adhesions via the traction stresses exerted by the cell on the extracellular matrix (ECM).^{6,13,26,34,39} However, there is a need to better understand the coupling of the global cell shape changes, the distribution of traction stresses and the associated biochemical processes.

Cell locomotion has been extensively studied using cell shape as readout. Wessels and Soll^{36,40} developed a framework for the 2D and 3D analysis of shape changes during cell locomotion, which enabled them to track the motion of amoeboid cells²⁰ through the observation of the time evolution of descriptors such as the cell length or the velocity of the cell centroid. Machacek and Danuser²⁵ identified different protrusion phenotypes using level set methods. Killich *et al.*¹⁹ and Keren *et al.*¹⁸ used Principal Component Analysis (PCA) (also known as Karhunen-Loève decomposition or Proper Orthogonal Decomposition) to quantify cell shape changes in migrating Dictyostelium cells and epithelial fish keratocytes. These studies employed a version of PCA that optimized the variance of the measured contour of the cell, to obtain a reduced set of dominant components of cell shape changes during migration. However, there is

Address correspondence to Juan C. Lasheras, Department of Mechanical and Aerospace Engineering, University of California, San Diego, 9500 Gilman Dr., La Jolla, CA 92093, USA. Electronic mail: lasheras@ucsd.edu

still the need to understand the dominant traction force patterns, and the associated biochemical processes, that the cell employs to produce mechanical work (energy) during migration.

Measuring the mechanical energy spent by the cell during migration requires having experimental access to the traction forces imposed by the cells on their ECM.⁴ Harris *et al.*¹⁴ identified qualitatively the nature of the stresses exerted by cells on the ECM through the observation of the wrinkling patterns cells induced over a thin layer of silicone rubber substratum. Dembo *et al.*¹¹ and Peterson²⁸ first described the use of elastic deformable substrates to measure the traction stresses exerted by cells attached to the substrate surface. This technique has since been applied to study the traction stresses exerted by different types of cells, including locomoting keratocytes,¹¹ fibroblasts²⁸ and Dictyostelium.^{10,23,26}

The objective of this work is to refine the spatio-temporal description of motility by obtaining a statistically significant characterization of the relationship between traction forces and cell shape in migrating amoeboid cells, using PCA as primary tool. For this purpose, we carried out simultaneous measurements of the time evolution of cell shape and traction forces exerted by isolated Dictyostelium cells undergoing chemotactic migration over a flat elastic substrate. In order to provide a physically relevant description, we applied a modified version of PCA to the measurements of the traction forces that optimized the strain energy accounted by each component. This analysis allowed us to determine the principal traction force patterns and shape changes implemented by migrating cells according to their importance for strain energy production. These patterns have a clear physical interpretation because the strain energy represents the amount of mechanical work performed by the cell against its surroundings while it is moving.

PCA effectively “compressed” the mechanics of migrating Dictyostelium cells by identifying a minimal set of traction force components that accounted the work performed by the cells. We found that the most important of these components accounted for ~40% of the traction work, and consists of a simultaneous contraction of the substrate from front and back towards the center of the cell. Its temporal evolution was oscillatory and correlated well with that of the strain energy and the cell length. In addition, we found that a set of five canonical principal components, exhibiting a high degree of repeatability from cell to cell, accounted for virtually all of the traction work exerted by WT cells. We also identified the most relevant principal components in two mutant strains with contractility defects: MyoII Essential Light Chain Null (mlcE⁻) and MyoII Heavy Chain Null (mhcA⁻) cells and compared it to the dominant components in WT.

The identification of a single most relevant component that accounts for a large portion of the strain energy opens new venues to develop semiempirical modeling approaches^{3,27,32,33} to describe the motion of the cell.

MATERIALS AND METHODS

Dictyostelium Culture and Microscopy

Axenicly grown Dictyostelium wild-type (WT) and mutant cells were prepared for chemotaxis and seeded onto a flat elastic gelatin gel as described previously.^{10,26} Time-lapse sequences of chemotaxing cells were acquired on an inverted microscope controlled by Metamorph software (Molecular Devices, Downingtown, PA).

Cell Shape Segmentation

Cell outlines were determined from differential interference contrast microscopy images using standard segmentation techniques.¹⁰

Traction Cytometry Experiments

The traction stresses exerted by cells were determined from measurements of the substrate deformation after solving the equation of static equilibrium for a linearly-elastic substrate in Fourier space, as described by del Álamo *et al.*¹⁰ (see Fig. 1a). The substrate deformation was obtained from the lateral displacements $\mathbf{u} = (u, v)$ of 0.1- μm fluorescent latex beads embedded in the gel. These displacements were measured by cross-correlating each instantaneous image with a reference image of the relaxed substrate.⁴¹ The Young's modulus of the gel was determined from the indentation of a tungsten carbide sphere.¹⁷ In the calculations, the tensile stresses at the free surface of the substrate were assumed to be negligible ($\tau_{zz}(z = h) \sim 0$), so that the stresses at the $z = h$ could be characterized by the 2D vector $\boldsymbol{\tau} = (\tau_{zx}, \tau_{zy})|_{z=h}$.

Cholesky Decomposition of the Strain Energy U_S Exerted on a Flat Substrate

The strain energy exerted by the cell on the surface of the substrate at a given instant of time was⁴

$$U_S(t) = \frac{1}{2} \int_A \boldsymbol{\tau}(\mathbf{x}, t) \cdot \mathbf{u}(\mathbf{x}, t) d\mathbf{x} = \{\boldsymbol{\tau}, \mathbf{u}\}, \quad (1)$$

where (\cdot) represents scalar product, $\int_A d\mathbf{x}$ represents a surface integral in a box enclosing the cell, and $\{\}$ represents an inner product. Note that U_S is equivalent

to the mechanical work the cell is exerts on the substrate.

We applied PCA to obtain a reduced set of traction force patterns which the cell used to exert mechanical work on the substrate. PCA works by optimizing the modal decomposition of a set of observations according to the norm associated to a predefined inner product. We then rewrote the strain energy as the norm $U_S = \{\theta, \theta\}$, where $\theta(\mathbf{x})$ is the strain energy square root or U_S -square root. This decomposition is called the Cholesky decomposition and is easier to perform in the Fourier domain,

$$U_S = \frac{L_B^2}{2} \sum_{\alpha=-\infty}^{\infty} \sum_{\beta=-\infty}^{\infty} \hat{\mathbf{u}}_{\alpha\beta}^* \cdot A_{\alpha\beta} \cdot \hat{\mathbf{u}}_{\alpha\beta}, \quad (2)$$

where $\hat{\mathbf{u}}_{\alpha\beta}$ are the Fourier coefficients of the lateral displacement vector, $A_{\alpha,\beta}$ is the Fourier norm matrix and $()^*$ denotes Hermitian transposition. In Fourier space, the problem of finding the functional Cholesky decomposition of the norm operator is reduced to finding the algebraic Cholesky decomposition of the norm matrix, $A_{\alpha\beta} = Q_{\alpha\beta}^* Q_{\alpha\beta}$, where $Q_{\alpha\beta}$ is a lower-triangular matrix. Introducing this decomposition in Eq. (2), one obtains that $\hat{\theta}_{\alpha\beta} = Q_{\alpha\beta}^* \hat{\mathbf{u}}_{\alpha\beta}$, and inversion of the Fourier transform yields

$$\theta(\mathbf{x}) = \mathcal{F}^{-1}(\hat{\theta}_{\alpha\beta}) = \mathcal{F}^{-1}(Q_{\alpha\beta}^* \hat{\mathbf{u}}_{\alpha\beta}). \quad (3)$$

Cell-based Coordinate System

Prior to applying PCA, we mapped the U_S -square root $\theta(\mathbf{x})$ in a non-dimensional cell-based coordinate system that took into account the changes in cell shape

and orientation (see Fig. 1b and del Alamo and co-workers^{10,26}). The origin of this coordinate system was the cell centroid, $(x_c(t), y_c(t))$, the coordinates were rescaled with the half-length of the cell, $L(t)/2$, and the axes were parallel to the principal axes of the cell. The coordinates in this cell-based reference system were

$$\begin{aligned} x^* &= [(x - x_c(t)) \cos \phi(t) + (y - y_c(t)) \sin \phi(t)] / [L(t)/2], \\ y^* &= [(y - y_c(t)) \cos \phi(t) - (x - x_c(t)) \sin \phi(t)] / [L(t)/2], \end{aligned} \quad (4)$$

where (x, y) were the coordinates in the laboratory reference frame, and $\phi(t)$ was the instantaneous angle between the longitudinal axis of the cell and the x -axis of the laboratory reference frame (see Fig. 1b). In order to ensure that the magnitude of both the traction forces and the strain energy were conserved upon transformation of reference frame, the traction stresses and the U_S -square root were redefined respectively as $\tau^*(\mathbf{x}^*) = L^2 \tau(\mathbf{x}^*)/4$ and $\theta^*(\mathbf{x}^*) = L \theta(\mathbf{x}^*)/2$. For simplicity, hereafter we will refer to \mathbf{x}^* as \mathbf{x} and to $\theta^*(\mathbf{x}^*)$ as $\theta(\mathbf{x})$. The size of the computational box where traction forces were calculated was 6 non-dimensional units, and was discretized using 129×129 nodes.

Scalar Field Mapping of Cell Shape Allows to Relate it to Traction Forces

The instantaneous cell shape is mapped using the non-dimensional cell-based coordinate system defined in Eq. (4) as a 2D function $d(\mathbf{x})$ such that $d(\mathbf{x}) = 1$ if \mathbf{x} laid within the contour of the cell, and $d(\mathbf{x}) = 0$ otherwise (Fig. 2a). This function was discontinuous at the contour of the cell, which could lead to undesired spurious oscillations in its modal decomposition (the

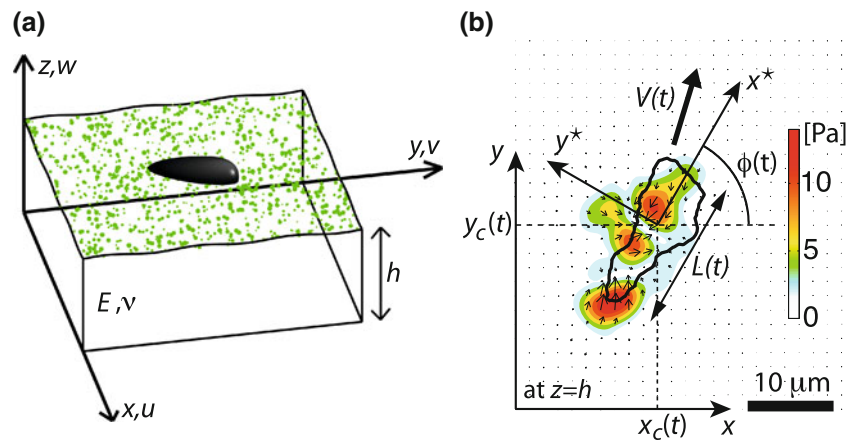


FIGURE 1. (a) Sketch representing a traction cytometry experiment. (b) Normalized cell-based reference system that adapts to the shape and orientation dynamics of the cell. The black contour is the cell outline. $L(t)$ is the cell length. (x, y) are the axes of the laboratory reference frame. (x^*, y^*) are the axes of the cell-based reference system, centered at the cell centroid $(x_c(t), y_c(t))$ and aligned with the principal axes of the cell, which are rotated an angle $\phi(t)$ with respect to (x, y) . The colormap indicates the strength of the traction stresses exerted by the cell on the substrate (Pa), and the arrows indicate their direction. The thick black arrow indicates the direction of motion of the cell, moving with velocity $V(t)$. Scale bar: $10 \mu\text{m}$.

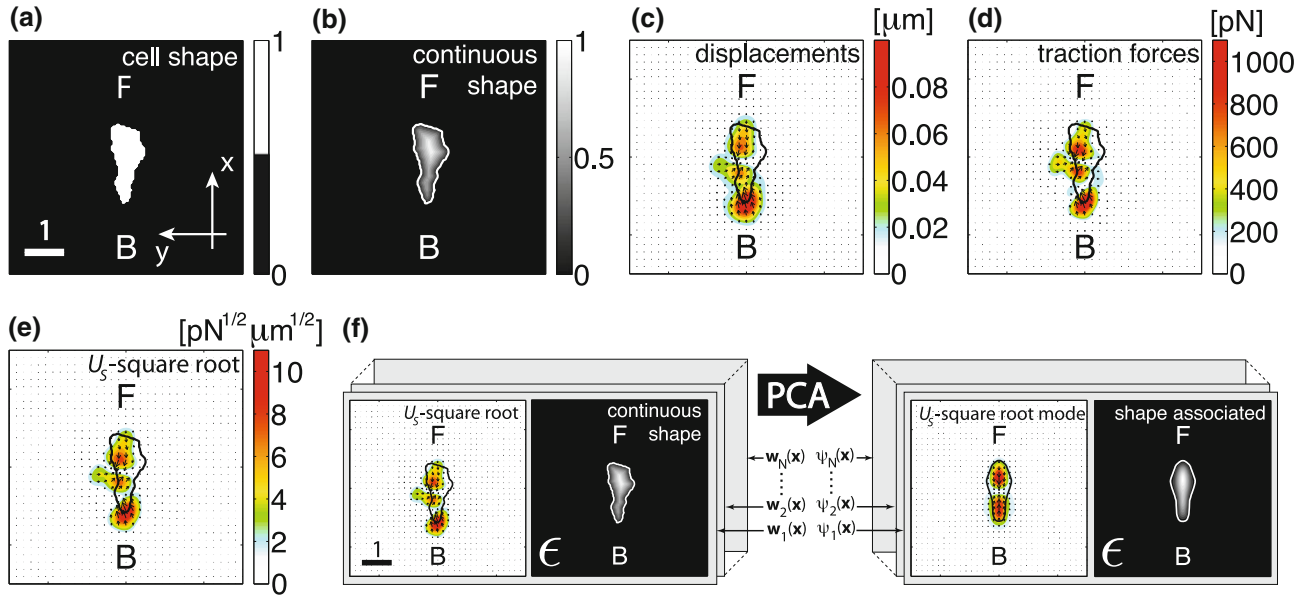


FIGURE 2. Representations used to study the dynamics of traction stresses and cell shape. For a WT cell at a certain instant of time: (a) 2D representation of the cell shape ($d(\mathbf{x})$). (b) 2D continuous representation of the cell shape ($s(\mathbf{x})$). The white line is the cell contour. At the free surface of the substrate: (c) Measured horizontal displacement field ($u(\mathbf{x})$), (d) Traction force field exerted by the cell ($\tau(\mathbf{x})$), (e) Strain energy square root ($\theta(\mathbf{x})$). In panels (c–e): the colormap and arrows indicate respectively the magnitude and direction of the variable represented, and the black contour is the cell outline. (f) We applied PCA over a set of observations combining $\theta(\mathbf{x})$ and $s(\mathbf{x})$ ($s(\mathbf{x})$ multiplied by a very small factor ϵ , so that its weight in the optimization process is negligible), and as a result we obtained a set of strain energy components ($\phi(\mathbf{x})$) and the cell shape associated to each component ($\chi(\mathbf{x})$). The scale bars in panels (a) and (f) indicate a half-length of the cell.

Gibbs phenomom, see Canuto *et al.*⁵), and deteriorates the convergence of PCA. This was avoided by using a continuous scalar field $s(\mathbf{x})$ to represent cell shape

$$s(\mathbf{x}) = d(\mathbf{x})c(\mathbf{x}) / \max_{\mathbf{x}}[c(\mathbf{x})], \quad (5)$$

where $c(\mathbf{x})$ was the distance from each point inside the cell \mathbf{x} to the cell contour (see Fig. 2b).

Because our aim was to determine how the cell shape associates with strain energy and traction forces at each instant of time, we applied PCA on the composite three dimensional function

$$\mathbf{w}(\mathbf{x}, t) = (\theta, \epsilon s)(\mathbf{x}, t), \quad (6)$$

which grouped both the U_S square root and the shape of the cell. The value of parameter ϵ was set very low ($\epsilon = 10^{-9} - 10^{-12}$) to ensure that the results from PCA only depended on the strain energy and were independent on shape variance. We verified that the use of the small parameter ϵ , as well as its selected magnitude, did not affect the calculation of the components of $\theta(\mathbf{x})$.

Principal Component Analysis (PCA) on the Strain Energy Square Root and Associated Cell Shape

Given a set of N experimental recordings of cell shape and traction forces (i.e. at times $t = t_k$ for

$k = 1 \dots N$), we applied PCA^{1,15} to the composite function $\mathbf{w}(\mathbf{x}, t)$ (Eq. (6)), which allowed us to express it as the weighted sum of principal components

$$\mathbf{w}(\mathbf{x}, t) = \sum_{k=1}^N a_k(t) \psi_k(\mathbf{x}), \quad (7)$$

where the basis functions $\psi_k(\mathbf{x}) = (\phi(\mathbf{x}), \epsilon \chi(\mathbf{x}))_k$, contain the spatial structure of cell shape and traction forces of each principal component and are denoted principal functions, and a_k is the weight coefficient of each component. To facilitate the interpretation of the principal functions, we transformed them into their traction force equivalents,

$$\xi(\mathbf{x}) = [2/\langle L \rangle] \mathcal{F}^{-1}(A_{\alpha\beta} Q_{\alpha\beta}^{T*-1} \hat{\phi}_{\alpha\beta})(\mathbf{x}), \quad (8)$$

where $\langle \rangle$ denotes temporal average and $\langle L \rangle$ is the average cell length.

The principal functions are mutually orthonormal with respect to the inner product (i.e. $\{\psi_i, \psi_j\} = 1$ if $i = j$ and zero otherwise), so that the total strain energy is given by

$$U_S(t) = \sum_{k=1}^N |a_k(t)|^2 = \sum_{k=1}^N U_S^k(t). \quad (9)$$

This property allows us to evaluate the instantaneous contribution of each term of the sum to the strain

energy, $U_S^k(t) = |a_k(t)|^2$. The time-averaged contribution of each component is usually referred to as the principal value associated to the component, λ_k . The principal components are arranged in decreasing order of λ_k , (i.e. $\lambda_{k+1} < \lambda_k$). The relative contribution of each principal component to the strain energy is obtained from the ratio $v_k = \lambda_k / \langle U_S \rangle$. The defining property of PCA is that, when applied to the U_S square-root (Eq. (3)), it distributes the maximum amount of strain energy in the fewest possible number of principal components.¹⁵

As a closing remark, we note that in many applications it is customary to subtract the average of the observations prior to performing PCA. This procedure is well suited for systems whose dynamics can be well represented as a fluctuating process superimposed on a steady state. However, this is not the case of chemotaxing amoeboid cells as previous studies have shown cell shape and traction forces show a marked periodic behavior in this type of cell migration.^{10,26} Thus, we applied PCA without subtracting the average of the observations, a procedure already reported in the literature,¹² and which in our case led to the maximization of the strain energy accounted for by each mode. We hypothesize that the dominant mode obtained by this procedure will capture the temporal periodicity of cell shape and traction forces. This hypothesis is tested in “One Principal Component Captures the Temporal Periodicity of Cell Length and Strain Energy During Amoeboid Cell Migration” section.

Individual and Ensemble PCA

We applied PCA to the time history of $\theta(\mathbf{x}, t)$ for 1) each single cell (individual PCA), and 2) for a pooled set of observations coming from all the cells recorded in our experiments (ensemble PCA). The high computational cost of performing ensemble PCA to all the cells (10468 observations from $N = 24$ cells) led us to consider 10 different sets, each of them containing 600 observations evenly distributed among each cell. Comparing the principal components obtained from individual and ensemble PCA allowed us to determine the cell-to-cell reproducibility of the principal components of shape and strain energy.

RESULTS

Traction Force Components in Wild-type Cells and Reproducibility

We applied PCA (see “Materials and Methods”) to determine the strain energy components exerted by WT Dictyostelium cells migrating chemotactically. The

five most energetic components were highly reproducible from cell to cell, allowing for their visual identification. Their spatial distributions are shown in Fig. 3. We will refer to them as the canonical principal components of the strain energy (CPCs). The reproducibility of these five components was proven by the fact that they were ranked as the dominant ones by ensemble PCA in all data pools analyzed (see Fig. 1 in the Supporting Material). Furthermore, “Five Principal Components Resolve the Spatio-temporal

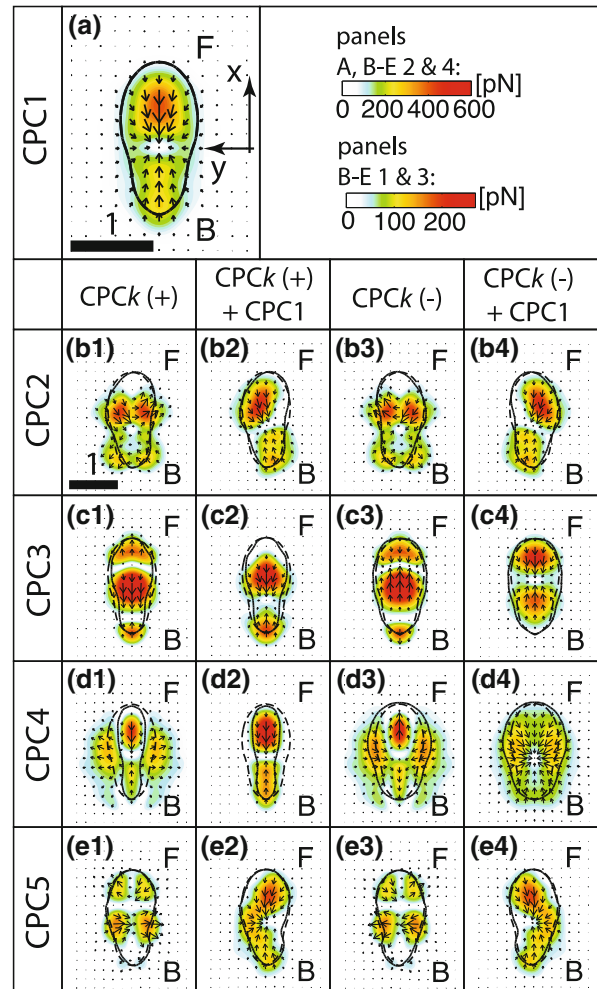


FIGURE 3. Canonical principal components of the strain energy (CPC) identified in WT cells. The panels in this figure represent the traction force generated through each strain energy component (Eq. (8)). The data come from one of the 10 pools of observations on which ensemble PCA was applied. CPC1 is represented in (a) and CPCk ($k = 2 - 5$) in (b-e). (b1/3-e1/3), (+)/(-) configuration of CPC2-5. (b2/4-e2/4), Overall effect of CPC2-5 (+)/(-) on CPC1. The colormap indicates the magnitude of the traction forces (pN). The solid black contour is the cell outline associated with each CPC. The dashed black contour indicates the median cell shape associated with component 1. Top-left corner: x and y are the non-dimensional axes for all panels. Scale bars: 1 non-dimensional unit of length = half-length of the cell. Labels “F” and “B” denote the front and back of the cell respectively.

Evolution of Traction Forces During Pseudopod Protrusion and Retraction” section shows that five principal components provided just enough time resolution to capture the evolution of the traction forces exerted by the cells during migration.

Altogether, the five CPCs accounted for $v_{1-5} \sim 60\%$ of the strain energy exerted by migrating, WT cells (Fig. 4), resulting in an average of 12% energy captured per mode. The narrow distribution of v_k for ensemble PCA suggested that each of the pools considered were representative of the whole cell line. Because our analysis employed time-lapse recordings containing 600 traction force maps (see “Individual and Ensemble PCA” section), PCA identified 600 strain energy components. The data in Fig. 4 indicate that the 595 components other than the CPCs account for remaining 40% of the strain energy exerted WT cells, leading to an average percent energy of 0.07%, which is 150 times lower than that of the CPCs.

The most important canonical principal component, CPC1, accounts for $\sim 40\%$ of the total strain energy exerted by WT cells (Fig. 4). Figure 3a displays CPC1 as $a_{1|50} \xi_1(\mathbf{x})$, where $\xi_1(\mathbf{x})$ is the traction force corresponding to CPC1 (see Eq. (8)) and $a_{1|50}$ is the median of its weight coefficient. CPC1 depicts the cell attaching at both its anterior and posterior parts and contracting the substrate inwards towards the centroid of

the cell. The coefficient a_1 , which modulated the magnitude of the traction forces in CPC1, was skewed towards positive values in 98.5% of the observations (see Fig. 5a), indicating that CPC1 accounted for a persistent contraction of the substrate from front and back. Unlike the first principal component, the weight coefficients of CPC2-5 were centered around zero (see Figs. 5b–5e). This result motivated the distinction between (+) and (–) configurations of these components (see Figs. 3b1–3e1 and 3b3–3e3). Because of both the high proportion of the strain energy U_S accounted for by CPC1 and the marked skewness of its weight coefficient towards positive values, it was useful to determine the perturbation effect that each CPCk ($k = 2 - 5$) had on the first principal component. Figures 3b2–3e2 display the addition of CPCk (+) to CPC1 as

$$a_{1|50} \xi_1(\mathbf{x}) + a_{k|90} \xi_k(\mathbf{x}), \quad (10)$$

and Figs. 3b4–3e4 display the addition of CPCk (–) to CPC1 as

$$a_{1|50} \xi_1(\mathbf{x}) + a_{k|10} \xi_k(\mathbf{x}) \approx a_{1|50} \xi_1(\mathbf{x}) - a_{k|90} \xi_k(\mathbf{x}). \quad (11)$$

The percentiles 10 and 90 of a_k were chosen to facilitate the visualization of the effect that CPC2-5 had in the overall traction force pattern, which was dominated by CPC1.

CPC2 and CPC5 were respectively responsible for $\sim 6\%$ and $\sim 3\%$ of the strain energy exerted by WT cells (Fig. 4) and accounted for lateral asymmetries in their traction forces. These components were associated with the bending of cell shape due to projection of pseudopods not aligned with the longitudinal axis of the cell (Figs. 3b and 3e, respectively). The overall effect of CPC2 (+)/(–) (Figs. 3b1/3b3) was to displace the region of application of traction forces towards the right/left at the back of the cell, and towards the left/right at the front. At the front, the cell shape displaced towards the right/left, not exerting significant forces, thus suggesting that the front was not attached. CPC5 (+)/(–) was similar to CPC2 (+)/(–), but presented an net enhancement of the contractile traction forces at the front (Figs. 3e2 and 4), which suggests that the front was attached to the substrate, in contrast to CPC2.

CPC3 was responsible for $\sim 6\%$ of the strain energy exerted by cells (Fig. 4). The (+)/(–) configuration of CPC3 depicted the contraction/stretch of the substrate from center to back and stretch/contraction of it from front to center (Figs. 3c1/3c3). The effect of CPC3 on the traction force pattern was easier to understand when added up to CPC1 (Figs. 3c2/3c4). CPC3 (+)/(–) displaced the areas of contraction of the substrate

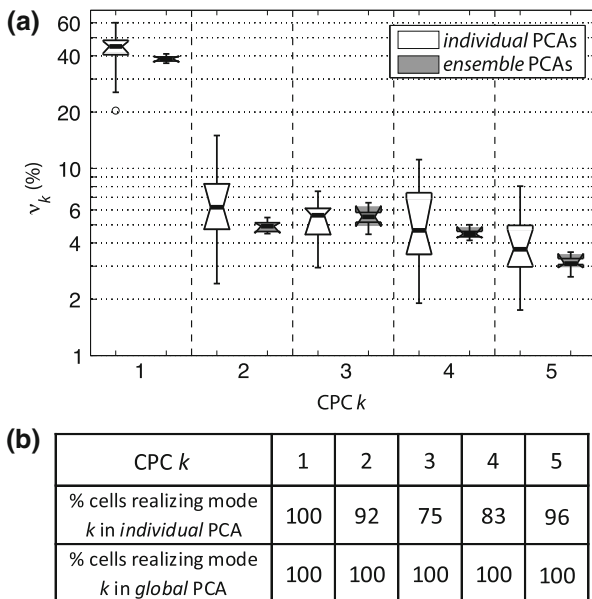


FIGURE 4. Contribution of each canonical principal component (CPC) to the total strain energy U_S for WT cells. (a) Boxplots of the fraction of U_S accounted for by each CPCk, v_k ($k = 1 - 5$), in individual and ensemble PCA. (b) Percentage of the cells (for individual PCA) and percentage of the pools of observations (for ensemble PCA) in which each CPCk was identified ($k = 1 - 5$). For individual PCA: $N = 24$ cells. For ensemble PCA: $N = 10$ pools of data with 600 observations each.

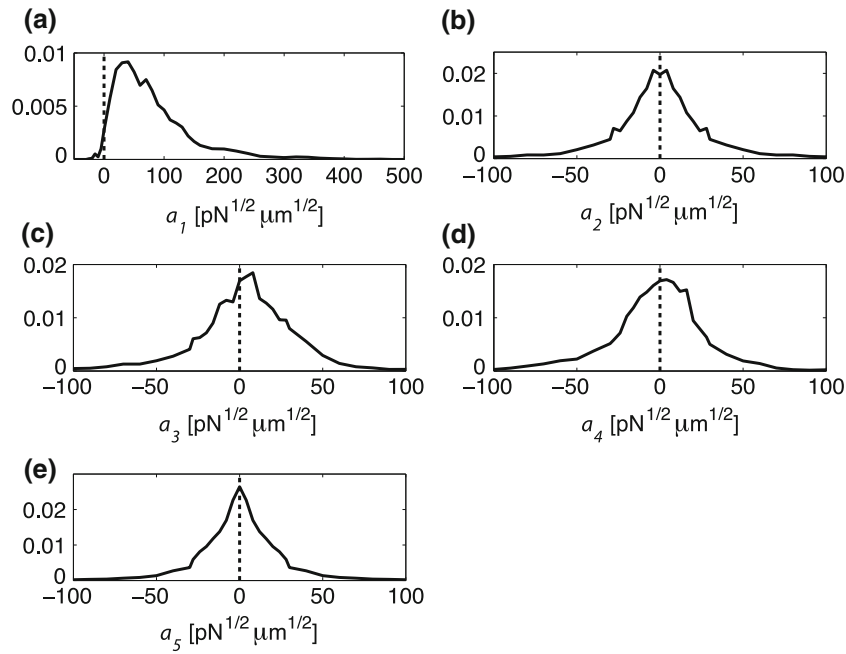


FIGURE 5. (a–e) PDF of the weight coefficients of each canonical principal component $\text{CPC}k$, a_k ($k = 1 - 5$), for the pool of all the observations ($N_{\text{observations}} = 10468$) coming from individual PCA applied over each WT cell ($N = 24$).

towards the back/front of the cell. The cell shape associated with CPC3 (+)/(-) was a slight elongation/dilation (see dashed black line in Fig. 3c).

CPC4 (Fig. 3d) accounted for $\sim 5\%$ of the total strain energy (Fig. 4). The (+)/(-) configuration of CPC4 accounted for an increase/decrease in the strength of the contractile forces at front and back, and a decrease/increase of the contractile lateral forces at the sides of the cell. CPC4 (+)/(-) was associated with the elongation/dilation of the cell shape.

One Principal Component Captures the Temporal Periodicity of Cell Length and Strain Energy During Amoeboid Cell Migration

Previous studies showed that U_S and L oscillate periodically and in phase during amoeboid cell migration,^{10,26} consistent with the cyclic implementation of anterior protrusions and posterior retractions by the cell.²⁰ In this section, we tested the hypothesis that these periodic oscillations had one degree of freedom and that they were controlled by the first CPC only. For this purpose, we analyzed the Spearman's rank correlation between the weight coefficient of $\text{CPC}k$, a_k , and either U_S or L ($r_{U_S-a_k}$ or r_{L-a_k} , $k = 1 - 5$), computed from individual PCA (see Fig. 6).

The PDF of $r_{U_S-a_1}$ was clearly displaced towards high positive values ($\langle r_{U_S-a_1} \rangle \sim 0.9$, $p < 10^{-5}$, Fig. 6b), indicating that, as we hypothesized, the temporal

evolution of U_S was accurately described by the temporal dynamics of CPC1. The weight coefficients a_k for components $k = 2 - 5$ showed no correlation with U_S , collapsing to zero for the asymmetric components $k = 2$ and 5. The PDF of r_{L-a_1} showed a statistically significant positive correlation ($p = 0.007$, Fig. 6c), which together with the high correlation between U_S and CPC1, indicates that the modulation of the inward contraction of the substrate from front and back of the cell was responsible for the positive correlation between U_S and L .^{10,26} Weight coefficient a_4 and L were also positively correlated ($p = 4 \times 10^{-5}$), due to the fact that CPC4 was an aspect ratio component that accounted for changes in traction forces related to the dilation and elongation of the cell (Eq. (4), Fig. 3d). The 2D-PDFs of a_k ($k = 2 - 5$) vs. a_1 (Fig. 7) showed that the weight of CPC2-5 was bounded by the weight of CPC1. This result confirmed that the first principal component governed the mechanics of amoeboid motility.

Five Principal Components Resolve the Spatio-temporal Evolution of Traction Forces During Pseudopod Protrusion and Retraction

In the previous section, we showed that the first CPC alone describes the periodic behavior of cell length and strain energy during migration. However, it is known that key events of cell migration are completed in shorter times than the full oscillations of U_S

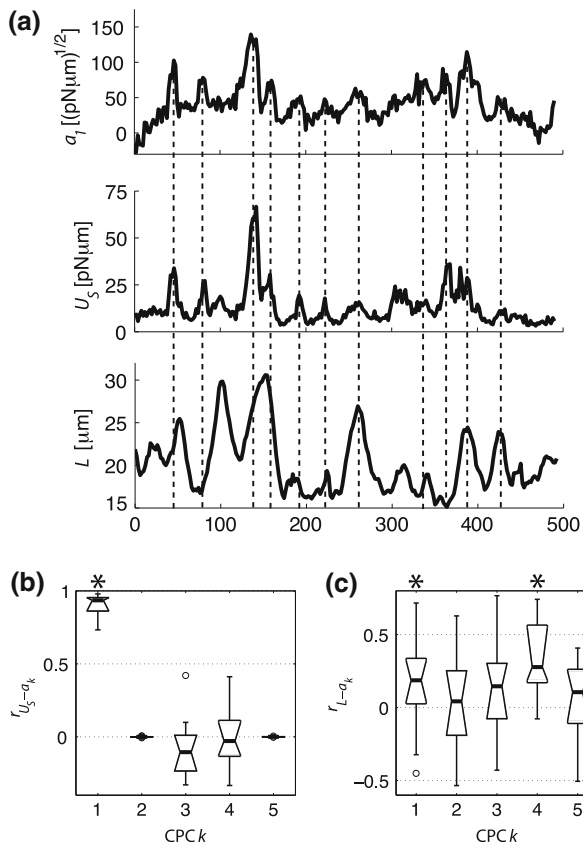


FIGURE 6. The weight coefficient of CPC1, a_1 , correlates with both the strain energy exerted U_S and the cell length L . (a) For a WT cell, temporal evolution of a_1 (top panel), U_S (middle panel), L (bottom panel). (b) Box-plot of the Spearman's rank correlation coefficient between the weight coefficient of the 5 CPCs identified, $a_k(t)$ ($k = 1 - 5$), and U_S . (c) Box-plot of the Spearman's rank correlation coefficient between $a_k(t)$ ($k = 1 - 5$) and L . Legend of the sign test of the null hypothesis that the statistical distributions in panels (a–b) have zero median: $*p < 0.01$.

and *L. Meili et al.*²⁶ reported that both pseudopod protrusion and retraction take on average ~ 22 s in chemotaxing WT cells, whereas the period of the oscillations in cell length was found to be ~ 94 s. This raised two questions: 1) does the first CPC provide enough temporal resolution to represent the mechanical stresses that cells exert on their substrate during migration? and 2) if not, how many CPCs are needed to obtain the required time resolution?

We estimated the temporal resolution of each principal component of the strain energy from the temporal memory of the weight coefficients obtained by individual PCA. That is, weight coefficients with long memory have a poor temporal resolution and *viceversa*. The temporal memory was quantified using the autocorrelation of the weight coefficients of each component, $R_{a_k}(\tau) = \langle a_k(t)a_k(t + \tau) \rangle$. We obtained a parabolic fit to the first 10 s of positive lag of R_{a_k} , and

calculated the time t_{R0} at which that parabola crossed the horizontal axis $R_{a_k} = 0$, providing with an estimated memory time for component k (Fig. 8a).

Figure 8b shows that the memory time decreased with the order of the principal component. In particular, the first CPC had a memory time $t_{R0}(k = 1) = 45$ s. The corresponding time resolution is too coarse to reproduce the dynamics of events such as protrusion or retraction, which have a duration of 22 s as reported by *Meili et al.* In order to determine how many principal components are required to resolve these events, we calculated the index k_{22} above which $t_{R0}(k)$ becomes < 22 s. Analysis of k_{22} revealed that five principal components are required to achieve a memory time of 22 s (Fig. 8c). Thus, we concluded that five principal components are needed to resolve the spatio-temporal evolution of traction forces during pseudopod protrusion and retraction.

Temporal Coordination Between Traction Forces and Lateral Protrusions

The two asymmetric canonical principal components, CPC2 and CPC5, were found to be associated with lateral protrusion of pseudopods. CPC5 accounts for the cell attaching the lateral protrusion to the substrate (Fig. 3b), whereas in CPC2 the lateral protrusion is not attached (Fig. 3b). The aim of this section was to analyze the possible temporal coordination between these two components, and how they are coordinated with the resulting bending of cell shape. The results from this analysis showed that the protrusion of lateral pseudopods takes about 12 s in average, starting with the lateral protrusion leading to the bending of cell shape and finishing with the attachment of the pseudopod to the substrate.

Application of PCA only to cell shape, similar to *Killich et al.*¹⁹ and *Keren et al.*,¹⁸ provided with a set of cell shape components. One of them accounts directly for cell bending and is temporally described by its weight coefficient $a_b^s(t)$. The PDFs of the Spearman's rank correlation coefficient between a_b^s and either a_2 or a_5 (Fig. 9b) proved that the association between cell shape bending and both CPC2 and CPC5 was positive and statistically significant. We studied the temporal coordination of cell shape bending, CPC2, and CPC5 through analysis of the cross-correlation of their weight coefficients and their temporal delays (Figs. 9a, 9c), showing that CPC5 is delayed ~ 12 s with respect to CPC2 ($p = 0.004$) (Figs. 9a, 9c, first boxplot) and that the physical bending of the cell precedes CPC5 by ~ 7 s ($p = 0.0015$) (Figs. 9a and 9c, second boxplot). Although Fig. 9c (third box-plot) suggests that CPC2 precedes the bending of the cell by ~ 4 s, the statistical significance was marginal ($p = 0.09$), probably

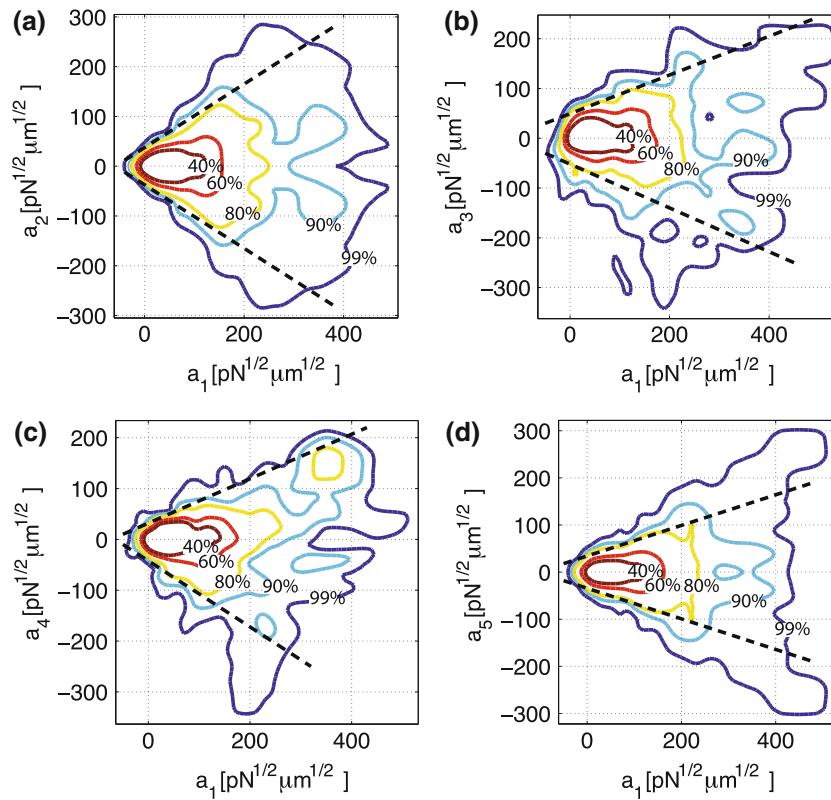


FIGURE 7. The weight of canonical strain energy components (CPC) 2–5 is bounded by the weight of CPC1. (a–e) 2D-PDFs of the weight coefficient of CPC k , $a_k(t)$ ($k = 2 - 5$), vs. the weight coefficient of CPC1, a_1 , for the pool of all the observations ($N_{\text{observations}} = 10468$) coming from individual PCA applied over each WT cell ($N = 24$). Solid lines represent the contours containing 40% (dark red), 60% (red), 80% (yellow), 90% (light blue) and 99% (blue) of the data. The dashed black lines indicate the approximate envelope of each 2D-PDF for $a_k - a_1$ ($k = 2 - 5$).

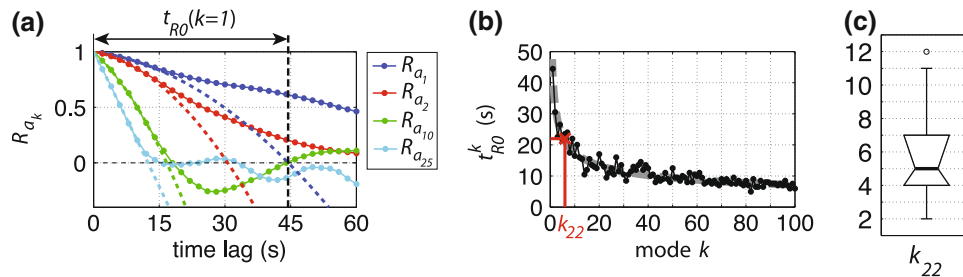


FIGURE 8. Temporal memory of the principal components in individual PCA. (a) —•—, autocorrelation of the weight coefficient of the strain energy components in a WT cell, R_{a_k} . Blue, $k = 1$; red, $k = 2$; green, $k = 10$; light blue, $k = 25$. — — —, parabola that fits R_{a_k} for time lag 0–10 s. The intersection of the parabola with the axis $R_{a_k} = 0$ determines the temporal memory of component k ($t_{R0}(k)$). (b) —•—, $t_{R0}(k)$ for the same cell. — — — (grey), the power law fit to $t_{R0}(k)$ (p_{R0}). The cross marks the component for which p_{R0} reaches 22 s (k_{22}), which is the temporal resolution needed to describe pseudopod protrusion and retraction.²⁷ (c) Box-plot of k_{22} for WT cells ($N = 24$).

because this delay was close to the temporal resolution of our experiments, 2 s.

Traction Force Components in Contractility Mutants are Similar to those in Wild-type Cells

To investigate the role that MyoII contractility plays in the strain energy components we applied PCA

to recordings of 1) MyoII essential light chain null cells with altered MyoII motor function⁷ ($mlcE^-$, $N = 13$), and 2) MyoII null cells lacking MyoII cross-linking and motor function³¹ ($mhcA^-$, $N = 19$).

Applying both ensemble and individual PCA (see “Materials and Methods”) to recordings of traction forces and cell shape for both $mhcA^-$ and $mlcE^-$ cells, we identified five CPCs for each mutant cell line.

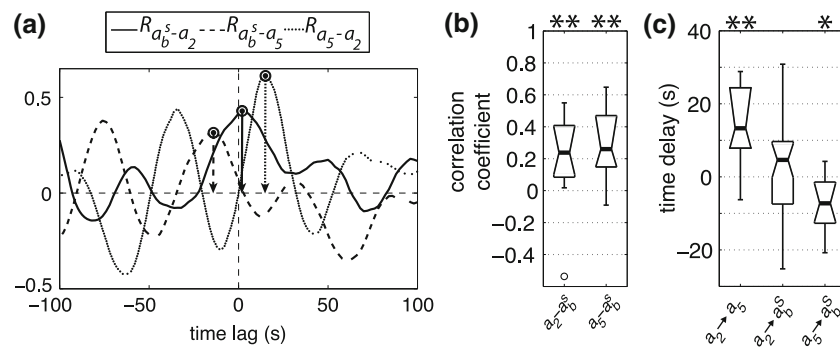


FIGURE 9. Analysis of the temporal coordination between cell shape bending and the two asymmetric canonical principal components of the strain energy, CPC2 and CPC5. (a) For a WT cell, cross-correlations between the bending of the cell (weight coefficient a_b^s), CPC2 (weight coefficient a_2) and CPC5 (weight coefficient a_5), used to quantify the delay between the signals (indicated with solid circles). (b) Box-plot of the Spearman's rank correlation coefficient between: a_2 and a_b^s , and a_5 and a_b^s . (c) Box-plot of the time delay, in s, between different weight coefficients, as extracted from their cross-correlations (see panel (a)) ($a_x \rightarrow a_y$ = time delay of a_y with respect to a_x). Stars indicate significance of testing the null hypothesis that the statistical distributions in panels (b–c) come from a continuous distribution with zero median: * $p < 0.05$ and ** $p < 0.01$.

These principal components, specially in $mlcE^-$, were remarkably similar to those identified for WT cells (Fig. 14 for $mlcE^-$, and 15 for $mhcA^-$ in the Supporting Material), and accounted for $\sim 55\%$ of U_S exerted by $mlcE^-$ and $mhcA^-$ (Fig. 13A in the Supporting Material).

As in WT cells, CPC1 accounted for a substantial proportion of the strain energy ($\sim 40\%$) in both $mlcE^-$ and $mhcA^-$ cells, indicating that temporal evolution of the mechanical interaction between contractility mutants and their substrate was also dynamically simple in these mutants. However, in $mhcA^-$ cells the principal components with $k > 1$ were less reproducible from cell to cell (Fig. 13C in the Supporting Material) than in WT, indicating the difficulty to define a clear “mechanical phenotype” for this cell line.

The first principal component in $mlcE^-$ was very similar to that in WT cells (Figs. 3a1, 10a), with traction forces focused at two areas at the posterior and anterior parts of the cell. However, this was not the case in $mhcA^-$ cells, where CPC1 presented a large amount of lateral forces (Fig. 10b). The prominent exertion of lateral forces by $mhcA^-$ is present throughout all the components (Fig. 15 in the Supporting Material).

DISCUSSION

Dr. Chien has been a major force in laying the foundation of mechanobiology, an emerging branch of cell biology that studies the interplay between mechanical forces and molecular biology. An essential element of mechanobiology is the variety of processes by which the cell responds to mechanical stresses, remodels its cytoskeleton and regulates its function in physiology and disease. Among his many

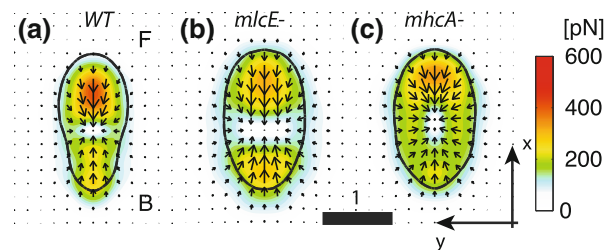


FIGURE 10. Traction force maps corresponding to the dominant canonical strain energy component (CPC1) in (a) WT, (b) $mlcE^-$ and (c) $mhcA^-$. The colormap and the arrows indicate the magnitude (in pN) and direction of the traction forces respectively. The solid black contour indicates the median cell shape associated with this component. See Eq. (8) for further explanation of the representation. x and y are the non-dimensional axes. Scale bar: 1 non-dimensional unit of length = half-length of the cell. Labels “F” and “B” denote the front and back of the cell respectively.

contributions, Dr. Chien has studied how external forces applied to the cell affect cell shape or cell migration.^{8,16,21,35,38,42} The present paper has been greatly inspired by Dr. Chien's pioneering work in this area.

In motile cells, shape changes are strongly related with the modulation of cell adhesions to the substrate via the forces they exert on it.^{6,13,26,34,39} In order to study this modulation, we measured the traction forces and cell shape of Dictyostelium cells migrating chemotactically over a flat elastic substrate. We then applied a tailored formulation of Principal Component Analysis (PCA) that optimized the mechanical work exerted by these cells. In addition, we used a 2D mapping of cell shape to obtain the different shape changes associated with each strain energy component.

Principal component analysis determined a set of five canonical principal components of the strain energy (CPCs) that were reproducible from cell to cell,

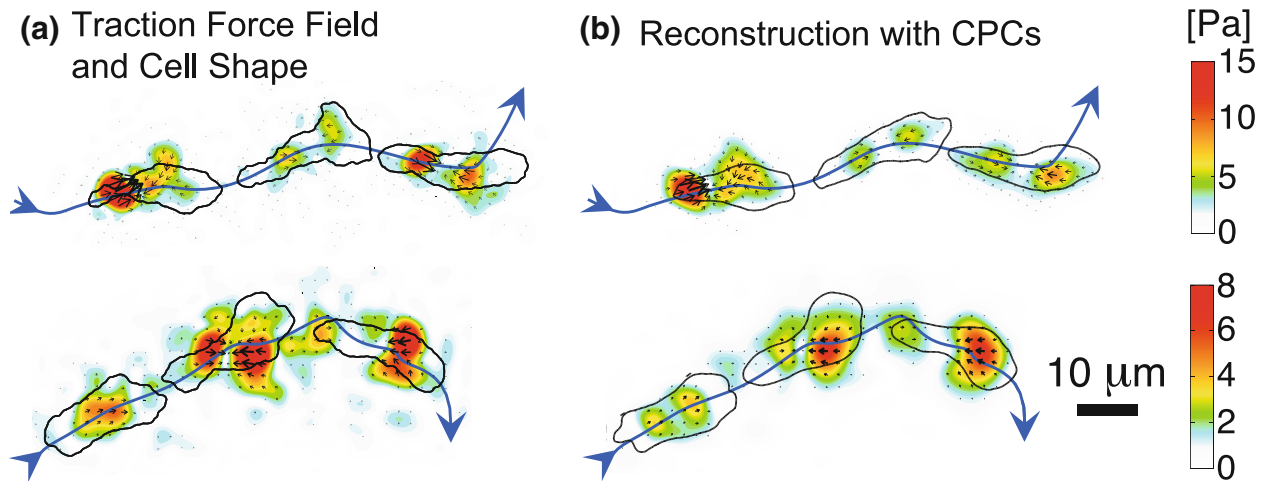


FIGURE 11. Comparison between instantaneous cell shape and traction force fields exerted by two chemotaxing cells (a) and reconstruction obtained with the 5 CPCs obtained from individual PCA (b). The colormap indicates the magnitude (colorbars in Pa) and the arrows the direction of the traction forces. The solid black contours represent measured (a) and reconstructed cell contours (b). The blue line indicates the cell trajectories, and the black bar is 10 μm long. Reconstructed cell contours were obtained as the contour of the reconstructed cell shape field function whose inscribed area equaled the instantaneous cell area.

and which captured $\sim 60\%$ of the total mechanical work exerted by cells. Furthermore, the five canonical components were shown to provide enough temporal detail to resolve the mechanics of pseudopod protrusions and retractions. This result opens a promising venue to the development of reduced models because it reveals that the complex dynamics of amoeboid cell migration can be encapsulated within the relatively simple dynamics of just five degrees of freedom. Figure 11 and Movie 1 in the Supporting Material illustrates this idea by comparing measurements of the time evolution of the shape and traction forces in a chemotaxing WT *Dictyostelium* cell with their projections onto the 5 CPCs. The agreement between the full measurements and the data obtained from the 5 CPCs is remarkable. Furthermore, the restriction to 5 CPCs reduces the noise of the traction force measurements.

The most important of these five components accounted for $\sim 40\%$ of U_S , presenting an oscillatory temporal evolution which correlated with both the strain energy and global cell shape. This dominant component depicted the cell attaching at front and back, contracting the substrate inward towards its center, and it is consistent with previous traction force measurements.^{10,23,26} The rest of the components were substantially less important in terms of mechanical energy, accounting for less than 7% each.

Keren *et al.*¹⁸ showed that a low number of components described the shape variability of migrating keratocytes within a population. In their cells, the most important component behaved steadily in time. Our study illustrates that PCA is also able to compress the more complex dynamics of amoeboid migrating cells

using a reduced number of degrees of freedom with coherent temporal evolution. For instance, our PCA identified two modes related with the initiation and termination of lateral protrusions. These components were separated by a period of ~ 12 s, during which an increase of traction forces revealed the formation of new adhesions.

The canonical principal components were found to be similar in the case of mutants with contractile deficiencies (*mlcE*⁻ and *mhcA*⁻), although these components were less reproducible in *mhcA*⁻ cells, indicating they have a less clear or less coherent “mechanical phenotype”. The first component in *mhcA*⁻ cells presented high lateral forces, suggesting the proliferation of lateral adhesions and cortical contractility as the origin of the traction forces in the absence of MyoII.

We have presented here the basics of an improved PCA analysis that allows for the dissection of cell motility into a reduced set of principal components. The application of this PCA method to mutant cell lines with adhesion, contractility, and actin polymerization defects represents a very attractive venue to improve our understanding on the role that the different cytoskeleton and adhesion proteins play in the generation of traction forces and the work needed for locomotion.

ELECTRONIC SUPPLEMENTARY MATERIAL

The online version of this article (doi:10.1007/s12195-011-0184-9) contains supplementary material, which is available to authorized users.

ACKNOWLEDGMENTS

This work was supported by grants USPHS 1RO1GM084227 and 3RO1GM037830.

REFERENCES

- ¹Berkooz, G., P. Holmes, and J. L. Lumley. The proper orthogonal decomposition in the analysis of turbulent flows. *Annu. Rev. Fluid Mech.* 25:539–575, 1993.
- ²Bray, D. *Cell Movements: From Molecules to Motility*, 2nd edn. New York: Garland Pub., pp. 41–58, 2001.
- ³Buenemann, M., H. Levine, W. J. Rappel, and L. M. Sander. The role of cell contraction and adhesion in dictyostelium motility. *Biophys. J.* 99(1):50–58, 2010.
- ⁴Butler, J. P., I. M. Tolic-Norrelykke, B. Fabry, and J. J. Fredberg. Traction fields, moments, and strain energy that cells exert on their surroundings. *Am. J. Physiol. Cell Physiol.* 282(3):C595–C605, 2002.
- ⁵Canuto, C., M. Y. Hussaini, A. Quarteroni, and T. A. Zang. *Spectral Methods: Fundamentals in Single Domains*. Scientific Computation, 1st edn. Berlin: Springer-Verlag, pp. 56–68, 2006.
- ⁶Chen, C. S., J. L. Alonso, E. Ostuni, G. M. Whitesides, and D. E. Ingber. Cell shape provides global control of focal adhesion assembly. *Biochem. Biophys. Res. Commun.* 307(2):355–361, 2003.
- ⁷Chen, T. L., P. A. Kowalczyk, G. Ho, and R. L. Chisholm. Targeted disruption of the Dictyostelium myosin essential light chain gene produces cells defective in cytokinesis and morphogenesis. *J. Cell. Sci.* 108(Pt 10):3207–3218, 1995.
- ⁸Chien, S. Mechanotransduction and endothelial cell homeostasis: the wisdom of the cell. *Am. J. Physiol. Heart C.* 292(3):H1209–H1224, 2007.
- ⁹Condeelis, J., and J. E. Segall. Intravital imaging of cell movement in tumours. *Nat. Rev. Cancer* 3(12):921–930, 2003.
- ¹⁰del Alamo, J., C. R. Meili, B. Alonso-Latorre, J. Rodriguez-Rodriguez, A. Aliseda, R. A. Firtel, and J. C. Lasheras. Spatio-temporal analysis of eukaryotic cell motility by improved force cytometry. *Proc. Natl Acad. Sci. USA.* 104(33):13343–13348, 2007.
- ¹¹Dembo, M., T. Oliver, A. Ishihara, and K. Jacobson. Imaging the traction stresses exerted by locomoting cells with the elastic substratum method. *Biophys. J.* 70(4):2008–2022, 1996.
- ¹²Ferreras, I., A. Pasquali, R. R. de Carvalho, I. G. de la Rosa, and O. Lahav. A principal component analysis approach to the star formation history of elliptical galaxies in compact groups. *Mon. Not. R. Astron. Soc.* 370(2):828–836, 2006.
- ¹³Gardel, M. L., B. Sabass, L. Ji, G. Danuser, U. S. Schwarz, and C. M. Waterman. Traction stress in focal adhesions correlates biphasically with actin retrograde flow speed. *J. Cell Biol.* 183(6):999–1005, 2008.
- ¹⁴Harris, A. K., P. Wild, and D. Stopak. Silicone rubber substrata: a new wrinkle in the study of cell locomotion. *Science* 208(4440):177, 1980.
- ¹⁵Holmes, P., J. L. Lumley, and G. Berkooz. *Turbulence, Coherent Structures, Dynamical Systems and Symmetry*, 1st edn. Cambridge Monographs on Mechanics. Cambridge: Cambridge University Press, pp. 86–128, 1996.
- ¹⁶Hsu, P. P., S. Li, Y. S. Li, S. Usami, A. Ratcliffe, X. Wang, and S. Chien. Effects of flow patterns on endothelial cell migration into a zone of mechanical denudation. *Biochem. Biophys. Res. Commun.* 285(3):751–759, 2001.
- ¹⁷Keer, L. M. Stress distribution at the edge of an equilibrium crack. *J. Mech. Phys. Solids* 12(3):149–163, 1964.
- ¹⁸Keren, K., Z. Pincus, G. M. Allen, E. L. Barnhart, G. Marriotti, A. Mogilner, and J. A. Theriot. Mechanism of shape determination in motile cells. *Nature* 453(7194):475–U1, 2008.
- ¹⁹Killich, T., P. J. Plath, E. C. Hass, W. Xiang, H. Bultmann, L. Rensing, and M. G. Vicker. Cell-movement and shape are nonrandom and determined by intracellular, oscillatory rotating waves in dictyostelium amoebae. *Biosystems* 33(2):75–87, 1994.
- ²⁰Lauffenburger, D. A., and A. F. Horwitz. Cell migration: a physically integrated molecular process. *Cell* 84(3):359–369, 1996.
- ²¹Li, S., P. Butler, Y. Wang, Y. Hu, D. C. Han, S. Usami, J. L. Guan, and S. Chien. The role of the dynamics of focal adhesion kinase in the mechanotaxis of endothelial cells. *Proc. Natl Acad. Sci. USA.* 99(6):3546–3551, 2002.
- ²²Li, S., J. L. Guan, and S. Chien. Biochemistry and biomechanics of cell motility. *Annu. Rev. Biomed. Eng.* 7:105–150, 2005.
- ²³Lombardi, M. L., D. A. Knecht, M. Dembo, and J. Lee. Traction force microscopy in dictyostelium reveals distinct roles for myosin ii motor and actin-crosslinking activity in polarized cell movement. *J. Cell. Sci.* 120(Pt 9):1624–1634, 2007.
- ²⁴Luo, L. Q. Rho gtpases in neuronal morphogenesis. *Nat. Rev. Neurosci.* 1(3):173–180, 2000.
- ²⁵Machacek, M., and G. Danuser. Morphodynamic profiling of protrusion phenotypes. *Biophys. J.* 90(4):1439–1452, 2006.
- ²⁶Meili, R., B. Alonso-Latorre, J. C. del Alamo, R. A. Firtel, and J. C. Lasheras. Myosin ii is essential for the spatio-temporal organization of traction forces during cell motility. *Mol. Biol. Cell* 21(3):405–417, 2010.
- ²⁷Mogilner, A., and B. Rubinstein. Actin disassembly ‘clock’ and membrane tension determine cell shape and turning: a mathematical model. *J. Phys. Condens. Matter* 22(19):194118, 2010.
- ²⁸Peterson, M. A. Theory of deformable substrates for cell motility studies. *Biophys. J.* 71(2):657–669, 1996.
- ²⁹Pollard, T. D., and G. G. Borisy. Cellular motility driven by assembly and disassembly of actin filaments. *Cell* 112(4):453–465, 2003.
- ³⁰Ridley, A. J., M. A. Schwartz, K. Burridge, R. A. Firtel, M. H. Ginsberg, G. Borisy, J. T. Parsons, and A. R. Horwitz. Cell migration: integrating signals from front to back. *Science* 302(5651):1704–1709, 2003.
- ³¹Robinson, D. N., and J. A. Spudich. Dynacortin, a genetic link between equatorial contractility and global shape control discovered by library complementation of a Dictyostelium discoideum cytokinesis mutant. *J. Cell Biol.* 150(4):823–838, 2000.
- ³²Rubinstein, B., K. Jacobson, and A. Mogilner. Multiscale two-dimensional modeling of a motile simple-shaped cell. *Multiscale Model. Simul.* 3(2):413–439, 2005.
- ³³Satulovsky, J., R. Lui, and Y. L. Wang. Exploring the control circuit of cell migration by mathematical modeling. *Biophys. J.* 94(9):3671–3683, 2008.
- ³⁴Sheetz, M. P., D. P. Felsenfeld, and C. G. Galbraith. Cell migration: regulation of force on extracellular-matrix-integrin complexes. *Trends Cell Biol.* 8(2):51–54, 1998.

- ³⁵Shiu, Y. T., S. Li, W. A. Marganski, S. Usami, M. A. Schwartz, Y. L. Wang, M. Dembo, and S. Chien. Rho mediates the shear-enhancement of endothelial cell migration and traction force generation. *Biophys. J.* 86(4):2558–2565, 2004.
- ³⁶Soll, D. R., D. Wessels, S. Kuhl, and D. F. Lusche. How a cell crawls and the role of cortical myosin ii. *Eukaryot. Cell* 8(9):1381–1396, 2009.
- ³⁷Springer, T. A. Traffic signals for lymphocyte recirculation and leukocyte emigration: the multistep paradigm. *Cell* 76(2):301–314, 1994.
- ³⁸Tzima, E., M. A. del Pozo, S. J. Shattil, S. Chien, and M. A. Schwartz. Activation of integrins in endothelial cells by fluid shear stress mediates rho-dependent cytoskeletal alignment. *EMBO J.* 20(17):4639–4647, 2001.
- ³⁹Wang, N., and D. E. Ingber. Control of cytoskeletal mechanics by extracellular-matrix, cell-shape, and mechanical tension. *Biophys. J.* 66(6):2181–2189, 1994.
- ⁴⁰Wessels, D., H. Vawter-Hugart, J. Murray, and D. R. Soll. Three-dimensional dynamics of pseudopod formation and the regulation of turning during the motility cycle of dictyostelium. *Cell Motil. Cytoskel.* 27(1):1–12, 1994.
- ⁴¹Willert, C. E., and M. Gharib. Digital particle image velocimetry. *Exp. Fluids* 10(4):181–193, 1991.
- ⁴²Zhao, Y., S. Chien, and S. Weinbaum. Dynamic contact forces on leukocyte microvilli and their penetration of the endothelial glycocalyx. *Biophys. J.* 80(3):1124–1140, 2001.